Icarus 314 (2018) 35–49

Contents lists available at ScienceDirect

Icarus

journal homepage: www.elsevier.com/locate/icarus

Expected precision of Europa Clipper gravity measurements

Ashok K. Verma[a,*], Jean-Luc Margot[a,b]

[a] Department of Earth, Planetary, and Space Sciences, University of California, Los Angeles, CA 90095, USA
[b] Department of Physics and Astronomy, University of California, Los Angeles, CA 90095, USA

ARTICLE INFO

Article history:
Received 1 February 2018
Revised 1 May 2018
Accepted 22 May 2018
Available online 26 May 2018

Keywords:
Europa
Geophysics
Tides, solid body
Satellites, shapes
Orbit determination

ABSTRACT

The primary gravity science objective of NASA's Clipper mission to Europa is to confirm the presence or absence of a global subsurface ocean beneath Europa's Icy crust. Gravity field measurements obtained with a radio science investigation can reveal much about Europa's interior structure. Here, we conduct extensive simulations of the radio science measurements with the anticipated spacecraft trajectory and attitude (17F12v2) and assets on the spacecraft and the ground, including antenna orientations and beam patterns, transmitter characteristics, and receiver noise figures. In addition to two-way Doppler measurements, we also include radar altimeter crossover range measurements. We concentrate on ± 2 h intervals centered on the closest approach of each of the 46 flybys. Our covariance analyses reveal the precision with which the tidal Love number k_2, second-degree gravity coefficients $\bar{C}_{20}$ and $\bar{C}_{22}$, and higher-order gravity coefficients can be determined. The results depend on the Deep Space Network (DSN) assets that are deployed to track the spacecraft. We find that some DSN allocations are sufficient to conclusively confirm the presence or absence of a global ocean. Given adequate crossover range performance, it is also possible to evaluate whether the ice shell is hydrostatic.

1. Introduction

The spacecraft mission design process at NASA relies on design requirements that flow from measurement requirements, which themselves flow from science objectives. The Europa Clipper mission has a set of compelling science objectives (e.g., Pappalardo et al., 2017) that emerged out of strategic planning documents (e.g., National Research Council, 1999, 2011) and other studies. Here we investigate some of the measurement requirements that may be needed to enable a gravity science investigation. Gravity science experiments provide powerful data for investigating the physical state of planetary bodies. Examples include mapping the gravity field, estimating the rotational state, and probing the internal structure of Mercury (e.g., Smith et al., 2012; Mazarico et al., 2014; Verma and Margot, 2016), Venus (e.g., Sjogren et al., 1997; Konopliv et al., 1999), Mars (e.g., Smith et al., 1999; Konopliv et al., 2011), and Titan (e.g., Iess et al., 2010).

In 2015, NASA appointed a Gravity Science Working Group (GSWG) to help refine science objectives for the Europa Clipper mission (then known as the Europa Multiple Flyby Mission). NASA's charge to the GSWG included the following statement: "The GSWG will define and recommend to the science team science investigations related to understanding the response of the satellite to gravity, specifically, but not limited to, understanding the tidal distortion of Europa, its internal structure, precession, and moments of inertia." The GSWG produced a report (Gravity Science Working Group, 2016) that specifies the precision with which certain quantities must be measured in order to meet specific science objectives (Table 1). The GSWG focused primarily on measurements that pertain to the ice shell and the presence of an ocean.

One of the primary objectives of a mission to Europa is to confirm the presence of a global ocean. A gravity science investigation can address this objective in a number of ways (Gravity Science Working Group, 2016). Here, we focus on measurements of the tidal Love number k_2. An alternate approach consists of measuring the tidal Love number h_2, as examined by Steinbrügge et al. (2018). Calculations by Moore and Schubert (2000) indicate that k_2 is expected to range from 0.14 to 0.26, depending on the thickness and strength of the ice shell, if a global ocean is present underneath the ice shell. In contrast, k_2 is expected to be less than 0.015 if there is no global ocean. Therefore, a measurement of k_2 is sufficient to test the global ocean hypothesis (Park et al., 2011, 2015; Mazarico et al., 2015), provided that the uncertainties do not exceed the 0.06 level recommended by the GSWG.

Another important objective of a gravity science investigation is to confirm whether the ice shell is in hydrostatic equilibrium.

* Corresponding author.
E-mail address: ashokverma@ucla.edu (A.K. Verma).

https://doi.org/10.1016/j.icarus.2018.05.018
0019-1035/

Table 1
A subset of possible measurement objectives for a Europa Clipper gravity science investigation (Gravity Science Working Group, 2016). The rightmost column specifies the one-standard-deviation precision with which geophysical parameters must be measured in order to meet gravity science objectives. The GSWG recommended multiplying formal uncertainties of fitted parameters by a factor of two to arrive at realistic one-standard-deviation uncertainties – see Section 4.4. The spherical harmonic coefficients in the representation of the gravity field are 4π-normalized. In this work, we focus on the first three objectives.

Objective	Quantity	Required precision
Confirm the presence of an ocean	Tidal Love number k	$k_2 < 0.06$
Verify whether ice shell is hydrostatic	Gravitational harmonics	$\bar{C}_{20} <$ 8e-6 and $\bar{C}_{22} <$ 9e-6
Measure shell thickness (to $\pm 20\%$)	Gravitational harmonics	$\bar{C}_{30} <$ 4e-7 and $\bar{C}_{40} <$ 4e-7
Confirm the presence of an ocean	Tidal Love number h	$h_2 < 0.3$
Confirm the presence of an ocean	Obliquity	$\theta < 0.01°$
Measure elastic shell thickness (to ± 10 km)	Tidal Love numbers	$k_2 < 0.015$ and $h_2 < 0.015$
Confirm ice shell is decoupled from interior	Amplitude of longitude libration	<50 m at tidal period

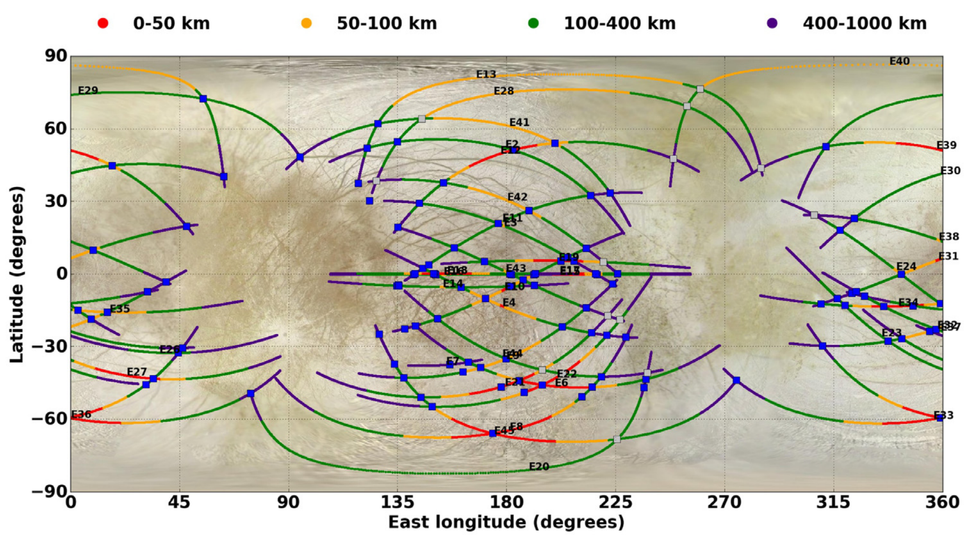

Fig. 1. Ground tracks (solid lines) and crossover locations (squares) corresponding to trajectory 17F12v2. Ground tracks are color-coded by altitude and crossovers are color-coded in blue (when Europa's surface is illuminated by the Sun) or silver (when the surface is in darkness). Only crossovers that occur when both altitudes are below 1000 km are shown.

Galileo-based estimates of second-degree gravity coefficients rely on the assumption of hydrostatic equilibrium (Anderson et al., 1998), but it is unclear whether hydrostatic equilibrium applies. It is possible to test the hydrostatic equilibrium hypothesis by measuring the second-degree gravitational harmonic coefficients, $\bar{C}_{20}$ and $\bar{C}_{22}$, to the level prescribed by the GSWG (Table 1). Trajectories being designed for the Clipper mission offer promising prospects for measuring these quantities.

In Section 2, we provide an overview of the anticipated Clipper trajectory. In Section 3, we review measurements, uncertainties, and model assumptions. Our dynamical model, solution strategy, and estimated parameters are discussed in Section 4. In Section 5, we discuss our covariance analysis results. Our conclusions are provided in Section 8.

2. Spacecraft trajectory and attitude

Europa Clipper will orbit Jupiter and execute repeated close flybys of Europa, Ganymede, and Callisto with science observations at Europa and gravitational assists at Ganymede and Callisto (Lam et al., 2015). To achieve the science goals of the mission, Clipper trajectories are designed to obtain globally distributed regional coverage of Europa with multiple low-altitude flybys (Pappalardo et al., 2017). The current trajectory, named 17F12v2, includes 46 flybys with altitudes as low as 25 km (Fig. 1) and 126 crossovers below 1000 km altitude. Crossovers are locations where two ground tracks intersect and where altimetric measurements are particularly valuable.

We examined the suitability of trajectories 15F10, 16F11, and 17F12v2 for gravity science investigations, with a particular emphasis on 17F12v2. All of these trajectories were designed to obtain globally distributed regional coverage of Europa with 42, 43, and 46 flybys, respectively (Table 2).

An important consideration for a gravity science investigation is the distribution of sub-spacecraft latitudes when the spacecraft is at closest approach. Trajectory 17F12v2 provides an adequate distribution for gravity science purposes (Table 3). Details about the spacecraft's anticipated trajectory and orientation in space (attitude) are available at ftp://naif.jpl.nasa.gov/pub/naif/EUROPACLIPPER in the form of SPICE kernels (Acton et al., 2017).

3. Measurements

The gravity science investigation will utilize a radio link between Earth-based stations and the spacecraft's radio frequency telecommunications subsystem to provide range and Doppler measurements (see Section 3.2) and solve for Clipper's trajectory. These data will yield measurements of Europa's gravity field and tidal response. The investigation will also rely on spacecraft-to-Europa ranging data from the Radar for Europa Assessment and Sounding: Ocean to Near-surface (REASON) instrument (Blankenship et al., 2014). Analysis of REASON data may be enhanced with digital elevation models obtained by stereo imaging from the Europa Imag-

Table 2
Characteristics of trajectories considered in this work: number of flybys according to closest approach altitude and number of illuminated crossovers with closest approach altitude below 1000 km.

Trajectory	Flybys				Illuminated crossovers
	<50 km	50–100 km	100–1000 km	>1000 km	<1000 km
15F10	22	15	1	4	88
16F11	26	13	2	2	106
17F12v2	25	16	2	3	112

Table 3
Definition of latitude regions and latitudinal distribution of flybys at the epochs of closest approach. The range of closest approach altitudes is also shown.

Europa region	Latitude range	Altitude range	Number of flybys
High latitude north	90° – 45°	25 km – 1442 km	9
Mid latitude north	45° – 15°	50 km – 100 km	4
Low latitude	15° – -15°	25 km – 100 km	13
Mid latitude south	-15° – -45°	25 km – 2554 km	12
High latitude south	-45° – -90°	25 km – 100 km	8

ing System (EIS) (Turtle et al., 2016). The primary observables will be two-way, coherent Doppler measurements (Section 3.2) and radar range measurements (Section 3.3). Our assumptions about the radio link and the Doppler and crossover measurements are summarized in Table 4 and explained in detail below.

3.1. Radio link

In order to meet mission requirements, it is anticipated that Clipper will carry at least three fan-beam (medium-gain) antennas and two wide-beam (low-gain) antennas. Nominal antenna gain patterns for these antennas were provided by Peter Ilott (pers. comm.) and Avinash Sharma (pers. comm.). We used these gain patterns in conjunction with the spacecraft attitude to compute the signal to noise ratio of the radio link. Clipper will carry a 20 W transmitter operating in the X band. Transmitter parameters were provided by Dipak Srinivasan (pers. comm.). Ground stations are expected to be primarily 34 m or 70 m antennas of the Deep Space Network (DSN) equipped with low-noise receivers. Nominal DSN system temperatures were provided by Ryan Park (pers. comm.). Typical spacecraft radio links are established in a closed-loop mode with a signal to noise ratio of 7 dB-Hz or above. A typical spacecraft radio link operates with a signal to noise ratio of 7 dB-Hz or above. However, it may be possible to use an open-loop receiver and obtain radio science data with a signal to noise ratio of 4 dB-Hz or less (Deep Space Network, 2016). However, it may be possible to establish a radio link with 4 dB-Hz. The DSN has the capability to array two or three 34 m antennas to improve the radio link budget.

3.2. Doppler measurements

Gravity science investigations rely primarily on two-way Doppler shift measurements between spacecraft and Earth-based antennas. These measurements yield the velocity of the spacecraft along the observer line-of-sight (LOS). Because the Doppler shift measures a component of the spacecraft velocity that is affected by the gravitational field, the radio tracking of spacecraft can produce detailed information about the distribution of mass in planetary bodies. To first order,

$$f_D \simeq 2 f_T \frac{V_r}{c}, \tag{1}$$

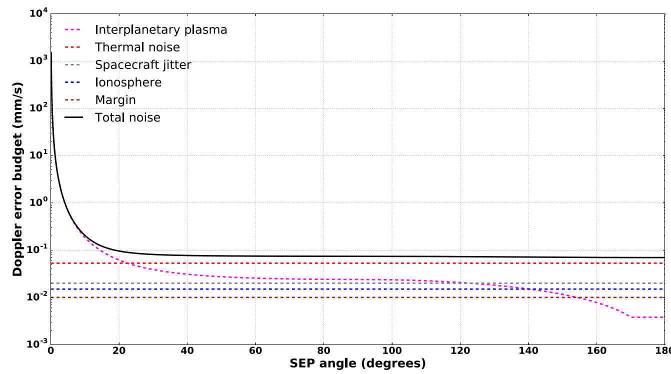

Fig. 2. Graphical representation of the Doppler error budget adopted in this work (Eq. (2)), showing Doppler uncertainties as a function of SEP angle. The model is appropriate for two-way Doppler measurements at X-band and 60 s integration time.

where f_D is the Doppler shift, f_T is the transmitted frequency, V_r is the LOS component of the relative velocity between spacecraft and observer, and c is the speed of light.

In this study, we assumed that the spacecraft telecom subsystem receives an X-band signal with a carrier frequency of ∼7.2 GHz from a DSN ground station and coherently transmits this signal back to the DSN with a carrier frequency of ∼8.4 GHz. The uncertainties of the Doppler measurements depend on a number of factors that include fluctuations in the ionospheric and solar wind plasmas, variations in the water content in the troposphere, as well as instrumental noise (Asmar et al., 2005). However, at small Sun-Earth-Probe (SEP) angles, the interplanetary plasma noise dominates. We modeled the Doppler uncertainties in a 60 s integration time as:

$$\sigma_D = \sqrt{\sigma_{plasma}^2 + \sigma_{other}^2} + 0.01 \text{ mm/s}, \tag{2}$$

where σ_{plasma} represents the noise due to interplanetary plasma according to the model of (Iess et al., 2012) and σ_{other} is a Europa Project estimate of the noise contribution due to other sources, including thermal noise (0.053 mm/s), spacecraft jitter (0.020 mm/s), and ionosphere (0.015 mm/s). The last term (0.01 mm/s) represents a margin added to the noise model (Fig. 2). See Asmar et al. (2005) for a detailed review of noise sources in radio science experiments.

3.3. Crossover measurements

Improvements to the quality of a spacecraft's orbit determination can be obtained when ranging measurements to a body of known shape and surface of known topography are available. Even when the shape varies with time and when the topography is unknown, as is the case for Europa, it is still possible to benefit from altimetry at so-called crossover points. Crossovers points are the geographic locations on the surface where two ground tracks intersect (Fig. 1). Ranges obtained at the same location on two separate

Table 4
Summary of assumptions regarding observables and radio science system.

Type	Assumption	Notes
Doppler measurements	X-band uplink	reference frequency $\sim$7.2 GHz
	X-band downlink	reference frequency $\sim$8.4 GHz
	60 s count time	integration time for Doppler measurements
	up to $\pm$2 h of tracking per flyby	centered on closest approach epochs
	0.07 mm/s $\leq \sigma_D \leq$ 0.096 mm/s	at 20° $\leq$ SEP $\leq$ 180°
	0.096 mm/s $\leq \sigma_D \leq$ 0.21 mm/s	at 10° $\leq$ SEP $\leq$ 20°
Crossover measurements	surface illumination by the Sun	excludes crossovers over non-illuminated terrain
	<1000 km altitude	spacecraft altitude at epochs of crossovers
	range uncertainties:	from REASON team
	median = 4.5 m	from REASON team
	standard deviation = 6.5 m	from REASON team
	[min, max] = [2.7, 24.9] m	from REASON team
Spacecraft transmitter and antennas	+40 dBm transmitter power	includes all losses due to waveguides and switches
	3 fan-beam antennas (FBAs)	orientation per 2c spacecraft model (Version 0.1)
	2 low-gain antennas (LGAs)	orientation per 2c spacecraft model (Version 0.1)
	LGAs: Gaussian beam pattern	peak at 7.5 dB and width of 42°
	FBAs: fan-beam pattern	$G(\theta, \varphi)$ from table lookup and bi-linear interpolation
	No obscuration by spacecraft structures	assumes free path, no scatter losses included
DSN antennas	68.4 dBi antenna gain	for 34 m antenna (NASA DSN, 2017)
	31.29 K system temperature	for 34 m antenna (from Ryan Park)
	74.3 dBi antenna gain	for 70 m antenna (NASA DSN, 2017)
	26.39 K system temperature	for 70 m antenna (from Ryan Park)
	1 Hz downlink loop bandwidth	used in noise power calculation
	2.71 dB two-antenna array gain	assumes typical 0.3 dB combining loss (NASA DSN, 2017)
	4.47 dB three-antenna array gain	assumes typical 0.3 dB combining loss (NASA DSN, 2017)
	Jupiter radio noise contribution	model from NASA DSN (2017); assumes 152 K black body
	No elevation or horizon mask	assumes continuous view of Jupiter by DSN assets
Radio link	Earth-Jupiter distance:	trajectory 17F12v2
	mean = 5.36 au	trajectory 17F12v2
	median = 5.39 au	trajectory 17F12v2
	[min, max] = [4.36, 6.28] au	trajectory 17F12v2
	4 dB-Hz link budget	best-effort basis

tracks can be subtracted to yield a crossover height difference:

$$\Delta h(t_1, t_2) = h(t_1) - h(t_2), \tag{3}$$

where $h(t)$ is the altimeter height measurement at time t. These crossover measurements eliminate the uncertainty introduced by the unknown local topography and can provide powerful constraints in the orbit determination process. The analysis of multiple crossover measurements obtained throughout Europa's orbital cycle will also be important in determining the radial amplitude of the tidal signal, i.e., in estimating the tidal Love number h_2 (e.g., Wahr et al., 2006).

To simulate crossover measurements, we assumed a nadir-pointed altimeter and incorporated spacecraft attitude data in our calculations. It is anticipated that the REASON instrument will range to the surface when the spacecraft is below altitudes of 1000 km with respect to the surface of Europa. We identified 126 crossovers with spacecraft altitudes < 1000 km in trajectory 17F12v2. However, 14 of these crossovers were discarded because they occur when the terrain under the spacecraft is not illuminated by the Sun during one or both of the encounters. Without proper illumination, it may not be possible to produce a Digital Terrain Model (DTM) from stereo analysis of EIS images. And without a DTM, the enhanced cross-over analysis approach that combines REASON and EIS data, as described by Steinbrügge et al. (2018), would not be possible.

We assigned uncertainties to the crossover measurements given by

$$\sigma_{t_1,t_2} = \sqrt{(\sigma_{t_1}^2 + \sigma_{t_2}^2)}, \tag{4}$$

where σ_t is the altimeter height measurement uncertainty at time t. These uncertainties were provided by the REASON team (Gregor Steinbruegge, pers. comm., Sept. 30, 2017) with heritage from the procedure described by Steinbrügge et al. (2018). The median and standard deviation of crossover uncertainties are 4.5 m and 6.5 m, respectively, with minimum and maximum values of 2.7 and 24.9 m, respectively.

4. Methodology

Our approach consisted in simulating the precision with which the Love number k_2 and degree-two gravitational harmonics can be determined with realistic mission scenarios and assumptions about measurement uncertainties (Section 3).

We used version 124 of the Mission Operations and Navigation Toolkit Environment (MONTE) (Evans et al., 2016), an astrodynamics computing platform that is developed at NASA's Jet Propulsion Laboratory (JPL). In addition to its uses in trajectory design and spacecraft navigation, MONTE has been used for a variety of scientific purposes, including gravity analysis (Verma and Margot, 2016), orbit determination (Greenberg et al., 2017), and sensitivity analysis for tests of general relativity (Verma et al., 2017).

MONTE's observation model uses Moyer (2003)'s formulation to compute Doppler measurements (Section 3.2) and a ray-intersect method to compute altitude measurements (Section 3.3). MONTE can specify arbitrary gravity fields (Section 4.1) and spin states (Section 4.2). We used MONTE's observation model to compute simulated observables and their partial derivatives with respect to solve-for parameters (Section 4.3). Finally, we used MONTE's tools to perform covariance analyses and quantify the precision with which geophysical parameters can be determined (Section 4.4). In the sections below, we provide details about the gravity and spin state models, solve-for parameters, and covariance analyses.

Table 5
Solve-for parameters and their a priori uncertainties used in covariance analyses.

Type	Parameter	A priori uncertainty	Number of parameters
Local	position	100 km	3 per flyby
	velocity	1 m/s	3 per flyby
	constant acceleration	5×10^{-11} km/s^2	3 per flyby
Global	GM	320 km^3/s^2	1
	Love number k_2	0.3	1
	20×20 gravity field	Kaula rule (see text)	437
	spin pole	1 °	2
	rotation rate	1×10^{-4} degree/day	1
Total			856

4.1. Representation of Europa's gravity field

MONTE represents gravity fields as spherical harmonic expansions (Kaula, 2000):

$$U = \frac{GM}{r} + \frac{GM}{r}\sum_{l=2}^{\infty}\sum_{m=0}^{l}\left(\frac{R}{r}\right)^{l}\bar{P}_{l,m}(\sin\varphi)\left(\bar{C}_{l,m}\cos(m\lambda) + \bar{S}_{l,m}\sin(m\lambda)\right), \tag{5}$$

where G is the gravitational constant, M is the mass of Europa, $\bar{P}_{l,m}$ are the normalized associated Legendre polynomials of degree l and order m, R is the reference radius of Europa (1562.6 km, Archinal et al. (2011)), and λ, φ, and r are the longitude, latitude, and distance of Clipper from the origin of the reference frame, which is chosen to coincide with Europa's center of mass. $\bar{C}_{l,m}$ and $\bar{S}_{l,m}$ are the 4π-normalized dimensionless spherical harmonic coefficients. In this work, we limited gravity field expansions to degree and order 20.

Jupiter's gravity field induces tides in Europa. Because of the small eccentricity of Europa's orbit, the tidal amplitude varies as a function of time. MONTE represents the tidal signal by applying time-varying corrections to the spherical harmonics coefficients (McCarthy and Petit, 2004, p.59):

$$\Delta\bar{C}_{2,m} - i\Delta\bar{S}_{2,m} = \left(\frac{k_{2,m}}{5}\right)\left(\frac{M_J}{M}\right)\left(\frac{R}{r_{EJ}}\right)^{3}\bar{P}_{2,m}(\sin\varphi_J)e^{-im\lambda_J}, \tag{6}$$

where $\Delta\bar{C}_{2,m}$ and $\Delta\bar{S}_{2,m}$ are the time-varying corrections to $\bar{C}_{2,m}$ and $\bar{S}_{2,m}$, respectively, $k_{2,\,m}$ is the Love number for degree 2 and order m, M_J is the mass of Jupiter, r_{EJ} is the distance between Jupiter and Europa, and λ_J and φ_J are the East longitude and latitude of the sub-Jupiter point in Europa's body-fixed frame. Here, we assume $k_{2,0} = k_{2,1} = k_{2,2} = k_2$.

4.2. Representation of Europa's spin state

The orientation of planetary bodies in inertial space can reveal important insights about interior properties. Europa's spin state is not know well. Its spin period is thought to be closely synchronized to its orbital period, and its obliquity is thought to be small (Bills et al., 2009). Analysis of existing Earth-based radar measurements is expected to provide a measurement of Europa's spin axis orientation to arcminute precision (Margot et al., 2013).

The orientation of Europa can be modeled as:

$$\alpha = \alpha_0 + \dot{\alpha}\Delta t + \sum_i A_i \sin M_i, \tag{7}$$

$$\delta = \delta_0 + \dot{\delta}\Delta t + \sum_i B_i \sin M_i, \tag{8}$$

$$W = W_0 + \dot{W}\Delta t + \sum_i C_i \sin M_i, \tag{9}$$

where α and δ are the right ascension and declination of the spin pole, respectively, W is the orientation of the prime meridian, α_0, δ_0, and W_0 are the values at the J2000 reference epoch, $\dot{\alpha}$, $\dot{\delta}$, and $\dot{W}$ are the corresponding rates of change, Δt is the time since the reference epoch, and the A_i, B_i, C_i, and M_i describe Fourier expansions of the nutation-precession and libration signatures. In this work, we use the rotation model that is recommended by the International Astronomical Union's Working Group on Cartographic Coordinates and Rotational Elements (Archinal et al., 2011), which has its origin in Lieske (1998)'s model. The values of the coefficients can be found in the current version (pck00010.tpc) of the planetary constants kernel published by NASA's Navigation and Ancillary Information Facility (NAIF) (Acton et al., 2017).

4.3. Solve-for parameters

In our simulations, we solved for the spacecraft's initial state vectors, unmodeled accelerations, and geophysical parameters of interest. We divided our solve-for parameters into two categories: *local* and *global*. The *local* parameters are applicable to a single flyby only, whereas the *global* parameters are common to all flybys. Each parameter was assigned an a priori uncertainty for the purpose of our covariance analyses (Table 5).

We placed a priori constraints on the uncertainties of coefficients of degree $l > 2$ in the expansion of the gravity field. The constraints follow a Kaula rule and we adopted the formulation given by Park et al. (2015):

$$K = \frac{(28 \times 10^{-5})}{l^2}\left(\frac{R_m}{R}\right)^{l}, \tag{10}$$

where K is the a priori constraint for coefficients of degree l and R_m is the assumed mantle radius of Europa (1465 km).

All *local* parameters are estimated for each flyby. The constant acceleration is necessary in order to account for unmodeled nongravitational forces (e.g., solar radiation pressure, Jupiter radiation pressure, etc.). Its components are expressed in the Radial-Transverse-Normal (RTN) frame associated with the spacecraft trajectory.

4.4. Covariance analysis

To evaluate the precision with which geophysical parameters of Europa can be determined, we performed covariance analyses (Bierman, 1977).

Given z observables and p solve-for parameters, the normal equations can be written as:

$$\eta = H^T W H + {C_0}^{-1}, \tag{11}$$

where H is the matrix of partial derivatives of z with respect to p, W is the matrix of weights appropriate for z, and C_0 is the a priori covariance matrix of p. We computed and stored the elements of the normal equations for all flybys, using 11,040 Doppler measurements, 112 crossover measurements, and 856 solve-for parameters. We computed the covariance matrix as:

$$C = \eta^{-1}. \tag{12}$$

The formal uncertainties in the estimated parameters are obtained by taking the square root of the diagonal elements of the covariance matrix:

$$\sigma_i = \sqrt{C_{ii}}. \tag{13}$$

The GSWG emphasized that formal uncertainties from covariance analyses are typically too optimistic, i.e., too small. The GSWG recommended multiplying formal uncertainties by a factor of 2 to arrive at more realistic one-standard-deviation uncertainties. In this work, we consistently multiplied formal uncertainties by a factor of 2 per GSWG recommendations. All uncertainty values listed or displayed have the factor of 2 applied.

The covariance analysis technique quickly enables the examination of a variety of scenarios. The normal equations are computed and stored once and for all. If one chooses to restrict the analysis to certain observables or certain parameters, one simply selects the relevant subset of lines and columns in η (Eq. (11)) and performs a new matrix inversion.

5. Results

We assumed that the spacecraft is tracked within ± 2 h of each closest approach, when the altitude of the spacecraft with respect to Europa's surface is $\leq$ 28,000 km. The radio link budget depends on the DSN assets that are deployed to track the spacecraft and on the spacecraft telecommunication assets, including antenna gain patterns. The Clipper spacecraft design currently includes two low-gain antennas and three medium-gain antennas. We assumed that Doppler measurements are available only when the radio link budget exceeds a nominal value (4 dB-Hz) that enables the establishment of a coherent, two-way link. Our calculations included the spacecraft position and attitude relevant to the 17F12v2 trajectory, variations due to spacecraft antenna gain patterns, occultations by Europa and Jupiter, and other assumptions listed in Table 4.

We examined two scenarios. In the first scenario, we assumed that one of the three most sensitive DSN antennas, the 70 m diameter antennas at Goldstone, Madrid, and Canberra, was used to track the spacecraft. This scenario reveals the best performance that one can hope to achieve with typical ground assets. In the second scenario, we assumed that 34 m diameter antennas were deployed either as single antennas or as arrays of antennas, and we examined the minimum set of assets that are necessary to meet the gravity science objectives.

We conducted three separate case studies in each of the two scenarios. In the first case study, we examined the precision that is achieved as the data from each consecutive flyby is processed. In the second case study, we asked how many flybys are necessary to meet the required measurement precision on k_2, $\bar{C}_{20}$, and $\bar{C}_{22}$ if the flybys tracked with DSN antennas are selected randomly from the set of all available flybys. In the third case study, we quantified the minimum number of flybys that are necessary to meet the measurement objectives when the flybys are grouped according to their sub-spacecraft latitude at closest approach. Results from these case studies allowed us to gain a progressively deeper understanding of the measurement precision that can be achieved in a variety of circumstances.

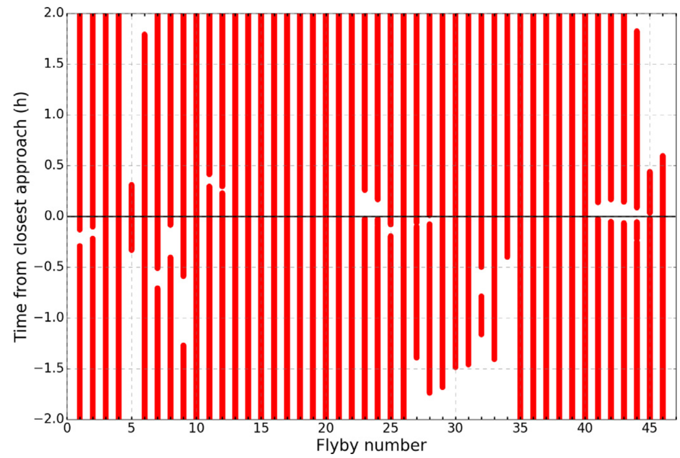

Fig. 3. Time intervals during which a 4 dB-Hz radio link can be maintained between 70 m antennas and Clipper on trajectory 17F12v2.

Table 6
Estimated uncertainties in closest-approach radial distances, tidal Love number k_2, and low-order gravity field coefficients with the 46 flybys of Case Study 1 in Scenario 1 (tracking Clipper on 17F12v2 trajectory with 70 m antennas). Entries in bold indicate that the requirements (rightmost column) were not met. Radial distance uncertainties include an indication of the spread (median ± standard deviation) across the 46 flybys.

Parameter	Doppler-only	Doppler+crossovers	Requirement
Radial distances	21 ± 57 m	19 ± 53 m	–
k_2	0.047	0.036	<0.06
$\bar{C}_{20}$	5.4×10^{-6}	4.1×10^{-6}	$<8.0 \times 10^{-6}$
$\bar{C}_{22}$	$\mathbf{9.2 \times 10^{-6}}$	7.0×10^{-6}	$<9.0 \times 10^{-6}$
$\bar{C}_{30}$	$\mathbf{7.1 \times 10^{-7}}$	$\mathbf{6.6 \times 10^{-7}}$	$<4.0 \times 10^{-7}$
$\bar{C}_{40}$	$\mathbf{7.3 \times 10^{-7}}$	$\mathbf{6.8 \times 10^{-7}}$	$<4.0 \times 10^{-7}$

5.1. Scenario 1: 70 m DSN antennas

In Scenario 1, we considered that 70 m DSN antennas were available for tracking, and we analyzed all 46 flybys of trajectory 17F12v2. After applying a 4 dB-Hz cutoff to the radio link budget, we were left with a total of 10,048 Doppler measurements (Fig. 3). We also considered up to 112 crossover measurements (Section 3.3). The exact number of Doppler and crossover measurements included in our analysis depends on the specific flyby selections in the various case studies.

We note that all flybys in 17F12v2 except E5 can be tracked for at least 1 h within ± 2 h of closest approach with a 70 m antenna. Flybys with less than 1 h of tracking time are problematic: they generally contribute little to the realization of measurement objectives and they have a high ratio of DSN overhead time to useful tracking time. Therefore, in this work, we focus on flybys that can be tracked for a total duration of at least 1 h (not necessarily continuous).

5.1.1. Case study 1: consecutive flybys

In this case study, we examined the precision of the estimates as data from consecutive flybys becomes available. At step n, the available observables consist of observables acquired during flybys 1 through n, and the solve-for parameters consist of global parameters and local parameters relevant to flybys 1 through n.

We conducted simulations for both Doppler-only and Doppler+crossover situations (Fig. 4). We found that measurement requirements for k_2 and $\bar{C}_{20}$ can be met (Table 6). The precision of the $\bar{C}_{22}$ gravity coefficient estimates in Doppler-only simulations does not meet the measurement objective. We found that $\bar{C}_{30}$ and $\bar{C}_{40}$ are never determined with sufficient precision to estimate the ice shell thickness at the $\pm 20\%$ level. The results

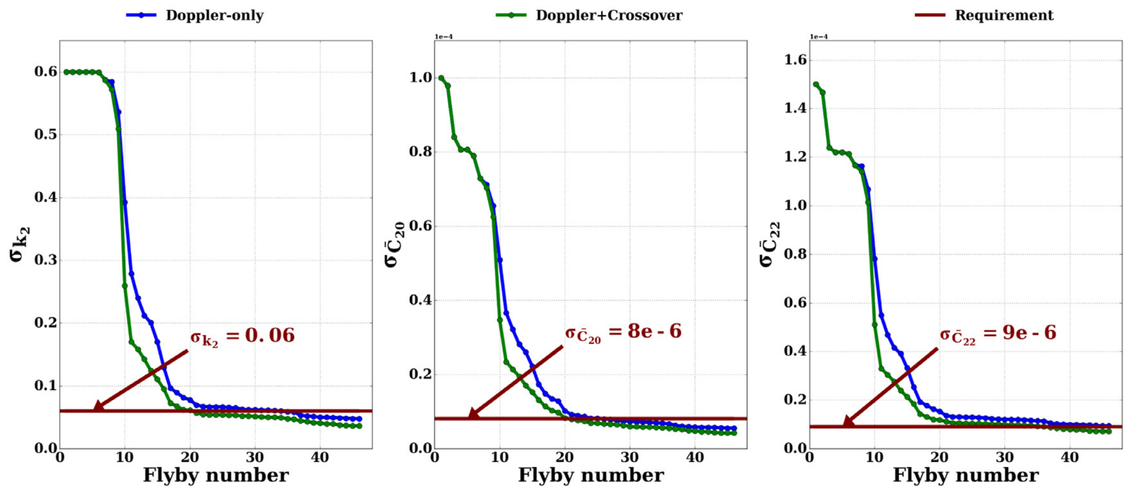

Fig. 4. Precision of the tidal Love number k_2 and gravity field coefficients $\bar{C}_{20}$ and $\bar{C}_{22}$ using Doppler (blue) and Doppler+crossover (green) measurements when data from 46 consecutive flybys tracked with 70 m antennas are analyzed (Scenario 1, Case Study 1). The brown horizontal lines indicate the measurement objectives specified in Table 1. (For interpretation of the references to colour in this figure legend, the reader is referred to the web version of this article.)

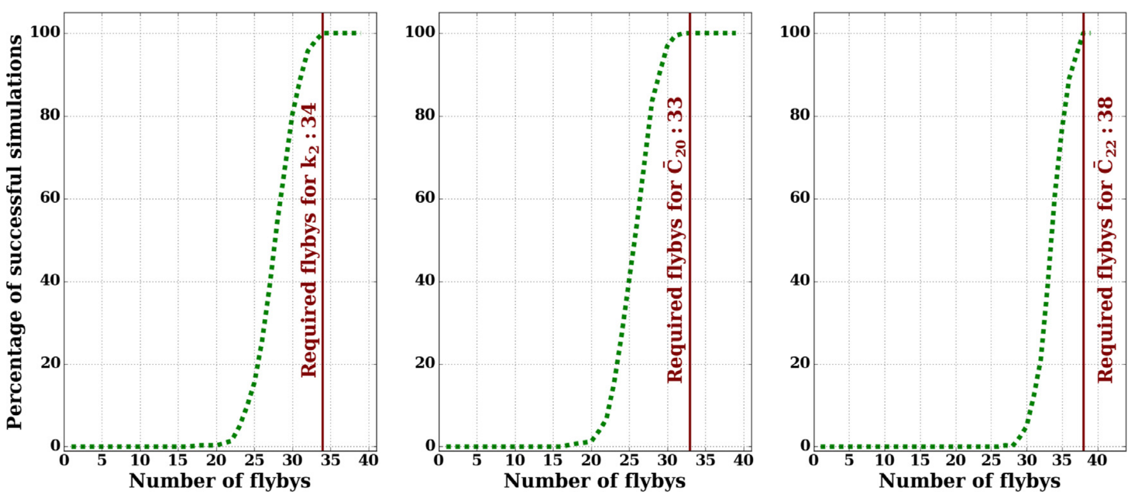

Fig. 5. Percentage of simulations that meet the tidal Love number k_2 and gravity field coefficients $\bar{C}_{20}$ and $\bar{C}_{22}$ measurement objectives, when considering up to 10,000 sets of randomly selected 17F12v2 flybys, as a function of the number of flybys considered in the sets (Scenario 1, Case Study 2). Simulations include both Doppler and crossover measurements and incorporate tracking of up to 39 flybys with a 70 m antenna, excluding high-altitude (>100 km) and low SEP (<20°) flybys.

indicate that k_2 and $\bar{C}_{20}$ measurement objectives can be met with fewer than 46 flybys, provided that tracking of the spacecraft is accomplished consistently with 70 m antennas. The results also demonstrate that measurement objectives can be achieved with fewer flybys when crossover measurements are included in the analysis.

5.1.2. Case study 2: random sets of flybys

In this case study, we quantified the minimum number of flybys that are necessary to meet measurement objectives when flybys tracked with DSN antennas are selected randomly from the set of available flybys. In actuality, DSN scheduling would likely take into consideration the flybys that provide the best possible science return. For this reason, we eliminated 4 flybys (E1, E25, E26, E46) that do not approach Europa's surface within 100 km and 3 flybys (E5, E6, E7) with SEP angles <20°. These seven flybys are expected to be less valuable than others from a gravity science perspective. Thus, we considered a maximum of 39 flybys in this case study. Because the previous case study revealed the value of combining Doppler and crossover measurements, we included both types of measurements in this case study.

Our simulations used a Monte Carlo scheme in which we considered n_c randomly selected flybys out of n_a available flybys (here, $n_a = 39$). The number of possible combinations is ($1 <= n_c <= 39$):

$$N = \frac{n_a!}{n_c!(n_a - n_c)!}. \tag{14}$$

If the number of combinations N was smaller than 10,000, we examined all possible combinations. Otherwise, we randomly selected 10,000 cases from the pool of available combinations. We gradually increased the number of considered flybys from 1 to 39. We found that it is possible to meet measurement objectives for k_2, $\bar{C}_{20}$, and $\bar{C}_{22}$ 100% of the time with 34, 33, and 38 flybys, respectively (Fig. 5).

An important goal of this case study was to gain information about the distribution of sub-spacecraft latitudes at closest approach that provides the best prospect of meeting measurement objectives. Based on our extensive set of simulations, we were able to quantify the number of flybys that are required according to specific latitude regions when considering sets of randomly selected flybys (Table 7).

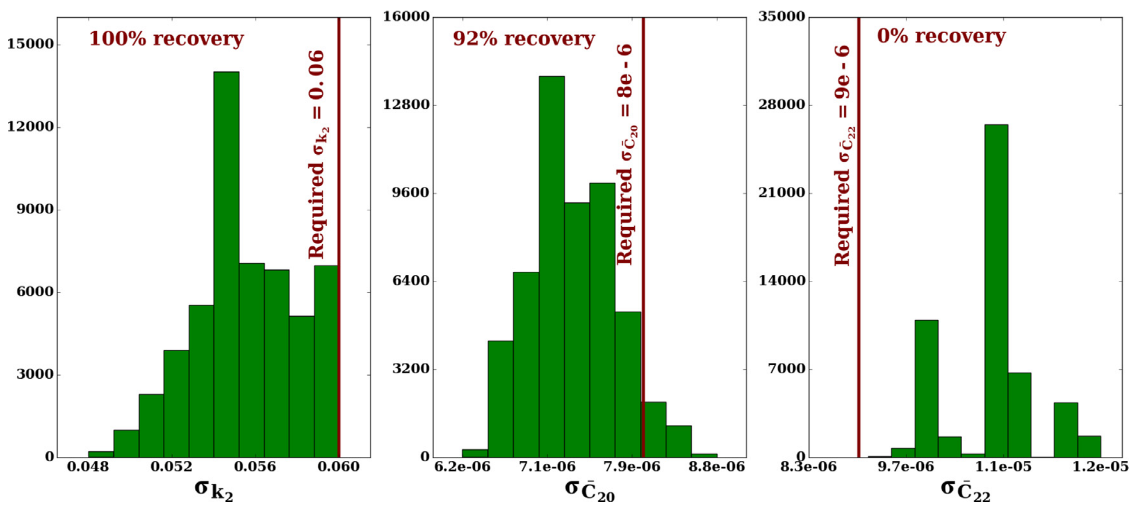

Fig. 6. Histograms of k_2, $\bar{C}_{20}$, and $\bar{C}_{22}$ uncertainties obtained by performing covariance analyses for all possible combinations of 23 flybys with the latitudinal distribution shown in Table 8 and tracking with 70 m antennas over time intervals shown in Fig. 3 (Scenario 1, Case Study 3).

Table 7
Observed latitudinal distribution of 17F12v2 flybys in successful simulations, i.e., in simulations where sets of randomly selected flybys always met the tidal Love number k_2 and $\bar{C}_{20}$ and $\bar{C}_{22}$ gravity field coefficients measurement objectives (Scenario 1, Case Study 2). Simulations include both Doppler and crossover measurements and incorporate tracking of up to 39 flybys with a 70 m antenna, excluding high-altitude (>100 km) and low SEP (<20°) flybys. The rightmost columns indicate the medians and standard deviations of the number of flybys that were included in successful simulations.

Europa region	Latitude range	Available flybys	k_2	$\bar{C}_{20}$	$\bar{C}_{22}$
High latitude north	90° – 45°	8	7 ± 1	7 ± 1	7 ± 0
Mid latitude north	45° – 15°	4	4 ± 1	3 ± 1	4 ± 0
Low latitude	15° – -15°	13	11 ± 1	11 ± 1	13 ± 1
Mid latitude south	-15° – -45°	8	7 ± 1	7 ± 1	8 ± 0
High latitude south	-45° – -90°	6	5 ± 1	5 ± 1	6 ± 0
Total	90° – -90°	39	34	33	38

5.1.3. Case study 3: preferred sets of flybys

In this third and final case study of Scenario 1, we used knowledge gained in previous case studies to inject some intelligence in the selection of flybys that can meet the primary (k_2) measurement objective. As in the previous case study, we discarded 7 flybys that either have low (< 20°) SEP angles or high (> 100 km) closest-approach altitudes. The remaining 39 flybys were classified into latitude regions. Because of the arrangement of the fan-beam (medium gain) antennas on the spacecraft, the low-latitude flybys are easiest to track with DSN assets. Thus, our selection started with all 13 low-latitude flybys. In the first step, we evaluated the performance with all 13 low-latitude flybys plus a randomly selected flyby from each mid-latitude band, for a total of 15 flybys. In the next step, we considered all 13 low-latitude flybys, a randomly selected flyby from each mid-latitude band, and a randomly selected flyby from each high-latitude band, for a total of 17 flybys. We gradually increased the number of mid- and high-latitude flybys in this fashion. At each step, we examined all possible combinations of flybys. We found that, with 70 m DSN assets, it is possible to meet the k_2 measurement objective with 23 methodically selected flybys (Table 8). Referring back to Fig. 5, about 10% of the simulations with 23 randomly selected flybys were successful with respect to k_2.

We evaluated k_2, $\bar{C}_{20}$, and $\bar{C}_{22}$ parameter uncertainties with the minimum number of flybys specified in Table 8. We performed covariance analyses for all possible combinations and found that it is possible to meet the k_2 measurement objective 100% of the time, whereas the requirements for $\bar{C}_{20}$ and $\bar{C}_{22}$ are met only 92% and 0% of the time, respectively (Fig. 6). It is possible to meet the $\bar{C}_{20}$ and $\bar{C}_{22}$ measurement objectives by increasing the number of flybys that are tracked (Section 5.1.2).

Table 8
Number of methodically selected 17F12v2 mid- and high-latitude flybys required to meet the tidal Love number k_2 measurement objective when flybys are tracked with 70 m DSN antennas and all low-latitude flybys are tracked (Scenario 1, Case Study 3).

Europa region	Latitude range	Avail. flybys	Req. flybys
High latitude north	90° – 45°	8	2
Mid latitude north	45° – 15°	4	3
Low latitude	15° – -15°	13	13
Mid latitude south	-15° – -45°	8	3
High latitude south	-45° – -90°	6	2
Total	90° – -90°	39	23

5.2. Scenario 2: minimum DSN assets

Scenario 1 provided estimates of what can be achieved with 70 m antennas. However, 70 m antenna time is difficult to schedule. In Scenario 2, we considered situations that place fewer demands on the ground telecommunication assets. We identified the minimal set of ground assets that achieve the k_2 measurement objective.

Similar to Scenario 1, we assumed that Doppler measurements were available only when the radio link budget exceeded 4 dB-Hz within ±2 h of each closest approach. One can deploy a variety of ground assets to maintain such a radio link. We considered

Table 9
Number of 17F12v2 flybys according to total (not necessarily continuous) tracking duration with a 4 dB-Hz link budget and various DSN assets.

DSN assets	Number of flybys		
	>4 h	1–4 h	<1 h
34 m	9	19	18
2×34 m	12	23	11
3×34 m	16	25	5
70 m	19	26	1

four configurations: a 34 m antenna, an array composed of two 34 m antennas, an array composed of three 34 m antennas, and a 70 m antenna. For each of these configurations, we computed the time intervals during which a 4 dB-Hz radio link can be maintained (Fig. 7).

We examined the distribution of flybys according to tracking duration with various DSN assets (Table 9). A 34 m antenna can track 9 flybys for ± 2 h of each closest approach. With a two-antenna or three-antenna array, the number of flybys that can be tracked increases to 12 and 16, respectively. A 70 m antenna can track 19 flybys for ± 2 h of each closest approach.

As in Scenario 1 (Section 5.1), we only considered flybys that provide the best possible science return. We therefore discarded 7 flybys either with high closest approach altitudes (>100 km) or low SEP angles (<20°). For the remaining 39 flybys, we identified the number of flybys for which Clipper can be tracked for at least 1 h (not necessarily continuous) within ± 2 h of closest approach with a link budget above 4 dB-Hz. We discarded flybys with less than 1 h of total DSN tracking because these flybys generally contribute little to the realization of measurement objectives and because of their high ratio of DSN overhead time to useful tracking time. A 34 m antenna is sufficient to track 26 out of the 39 considered flybys for more than 1 h. We label this configuration $\mathrm{DSN}_{34\mathrm{m}}$. If we combine two 34 m antennas into a two-antenna array, 5 additional flybys can be tracked for more than 1 h. The union of $\mathrm{DSN}_{34\mathrm{m}}$ and these 5 additional flybys yields a total of 31 flybys, a configuration that we label $\mathrm{DSN}_{2\times34\mathrm{m}}$. If we combine three 34 m antennas into a three-antenna array, 5 additional flybys can be tracked for more than 1 h. The union of $\mathrm{DSN}_{2\times34\mathrm{m}}$ and these 5 additional flybys yields a total of 36 flybys, a configuration that we label $\mathrm{DSN}_{3\times34\mathrm{m}}$. If a 70 m antenna is used, 3 additional flybys can be tracked for more than 1 h. The union of $\mathrm{DSN}_{3\times34\mathrm{m}}$ and these 3 additional flybys yields a total of 39 tracked flybys, a configuration that we label $\mathrm{DSN}_{70\mathrm{m}}$. The number of available flybys with each DSN configuration are summarized in Table 10, and the corresponding tracking coverage is illustrated in Fig. 8. In order to minimize the use of ground assets, we select, for each flyby, the least sensitive antenna configuration that can provide at least 1 h of tracking. Specifically, we do not use additional assets to extend the duration of flybys that are already tracked for at least 1 h (compare Fig. 7(d) to Fig. 8).

The available number of Doppler and crossover measurements varies according to the chosen DSN configuration (Table 11). However, the exact number of Doppler and crossover measurements included in our analysis depends on the specific flyby selections in the various case studies.

5.2.1. Case study 1: consecutive flybys

This Scenario 2 case study is based on the same principles as its analog in Scenario 1 (Section 5.1.1). We analyzed the Doppler and crossover data from consecutive flybys as it becomes available.

We found that measurement objectives cannot be met if tracking is restricted to a single 34 m antenna (Fig. 9). However, it is

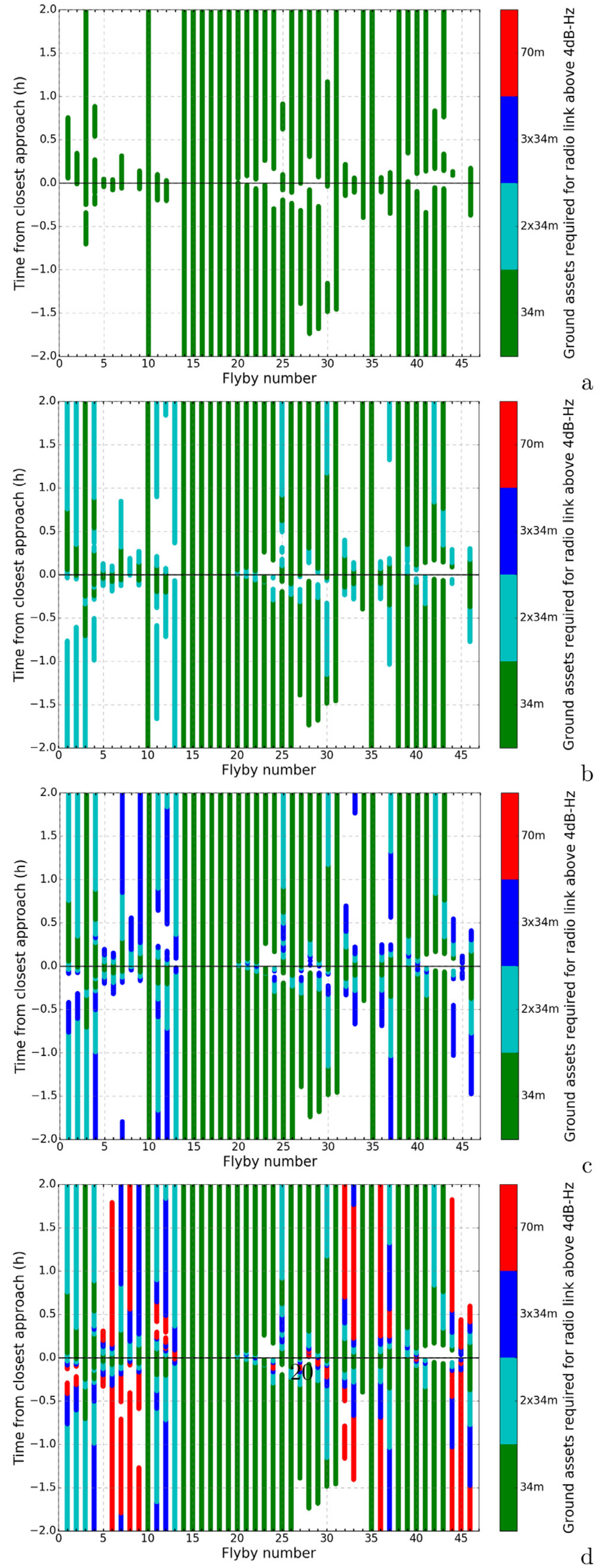

Fig. 7. Time intervals during which a 4 dB-Hz radio link can be maintained between Clipper and progressively more sensitive DSN assets: (a) a 34 m antenna, (b) two 34 m antennas, (c) three 34 m antennas, and (d) a 70 m antenna.

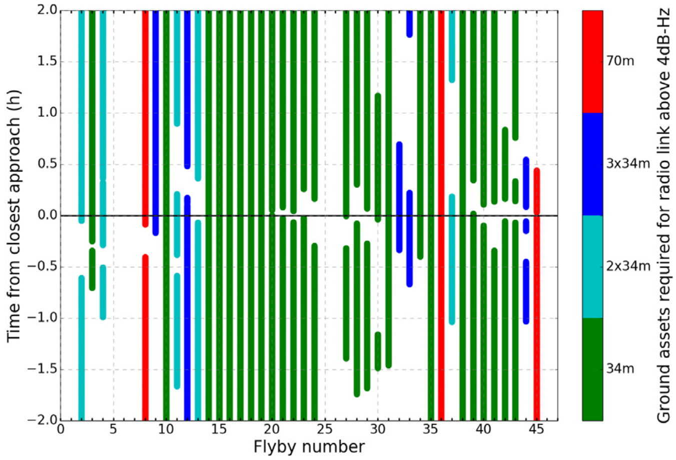

Fig. 8. Time intervals during which a 4 dB-Hz radio link can be maintained for at least 1 h. For each flyby, the least sensitive antenna configuration was used. Flybys with low SEP angles (<20°) or high altitudes (> 100 km) were discarded, leaving a total of 39 flybys. See also Table 10.

possible to meet the k_2 measurement objective with the $DSN_{2\times34m}$ configuration by tracking 26 flybys with a single 34 m antenna and 5 additional flybys with a two-antenna array (2×34 m), for a total of 31 tracked flybys.

The estimated uncertainties in tidal Love number k_2 and low-order gravity field coefficients using a variety of DSN assets are shown in Table 12. The measurement objective pertaining to verifying whether the ice shell is hydrostatic (Table 1) is barely met with the most sensitive antenna configuration. The gravity field coefficients $\bar{C}_{30}$ and $\bar{C}_{40}$ are never measured at the level required to measure the ice shell thickness with ±20% uncertainties (Section 1).

5.2.2. Case study 2: random sets of flybys

This Scenario 2 case study is based on the same principles as its analog in Scenario 1 (Section 5.1.2). We quantified the minimum number of flybys that are necessary to meet measurement objectives when tracked (>1 h) flybys are selected randomly from the set of available flybys.

Table 10
Number of 17F12v2 flybys that can be tracked (≥ 4 dB-Hz) for at least 1 h (not necessarily continuous, Fig. 8) within ±2 h of each closest approach for increasingly sensitive antenna configurations.

Configuration	Number of available flybys				Total
	34 m	2x34 m	3x34 m	70 m	
DSN_{34m}	26	...	...	...	26
$DSN_{2\times34m}$	26	5	...	...	31
$DSN_{3\times34m}$	26	5	5	...	36
DSN_{70m}	26	5	5	3	39

Table 11
Number of Doppler and crossover measurements that can be obtained with the antenna configurations listed in Table 10, compared to the numbers obtained when tracking 39 flybys with 70 m antennas. The number of crossovers corresponds to the number of intersections of tracked flybys. Also shown are the total durations during which tracking can be conducted with a link budget above 4 dB-Hz, expressed as a fraction of the total potential tracking time (±2 h of each closest approach, or 184 h in 17F12v2). Flybys with <1 h tracking duration, SEP angle <20°, and altitude >100 km were discarded.

DSN config.	Doppler msr.	Crossover msr.	Tracking fraction
DSN_{34m}	5503	37	50%
$DSN_{2\times34m}$	6371	62	58%
$DSN_{3\times34m}$	6922	84	63%
DSN_{70m}	7527	95	68%
Tracking of 39 flybys with 70 m antennas	8756	95	79%

Because it is not possible to meet science objectives with a single 34 m antenna (DSN_{34m}), we selected the $DSN_{2\times34m}$ antenna configuration, where a 2x34 m antenna array is used on up to 5 occasions to supplement the up to 26 flybys tracked with a single 34 m antenna. Thus, a total of up to 31 tracked flybys are available in this case study (Table 10).

We considered n_c randomly selected flybys out of n_a available flybys (here, $n_a = 31$). The number of possible combinations is given by Eq. (14). If the number of combinations N was smaller than 10,000, we examined all possible combinations. Otherwise, we randomly selected 10,000 cases from the pool of available combinations. We gradually increased the number of considered flybys from 1 to 31.

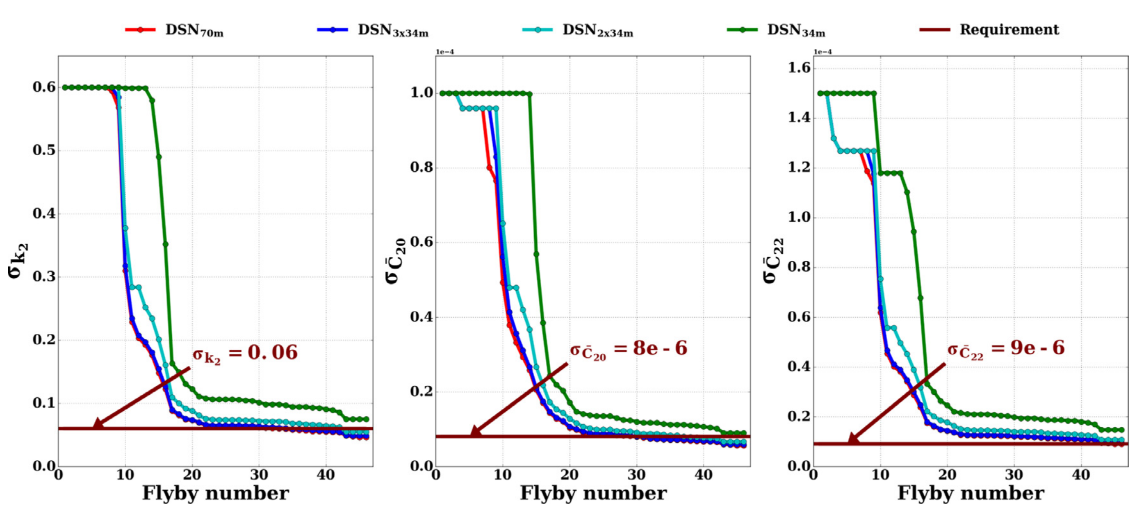

Fig. 9. Precision of the tidal Love number k_2 and gravity field coefficients $\bar{C}_{20}$ and $\bar{C}_{22}$ estimates when data from 46 consecutive flybys are analyzed (flybys with <1 h tracking duration, SEP angle <20°, and altitude >100 km were discarded) using progressively more sensitive DSN configurations (Scenario 2, Case Study 1, Table 10). The green curve shows the performance with 26 flybys tracked with a single 34 m antenna configuration (DSN_{34m}). The cyan curve considers the addition of a second antenna for 5 flybys, for a total of 31 flybys ($DSN_{2\times34m}$). The blue curve considers the addition of a third antenna for 5 flybys, for a total of 36 flybys ($DSN_{3\times34m}$). The red curve considers the addition of a 70 m antenna for 3 flybys, for a total of 39 flybys (DSN_{70m}). The red curve is nearly indistinguishable from the blue curve. The brown horizontal lines indicate the measurement objectives specified in Table 1.

Table 12
Estimated uncertainties in tidal Love number k_2 and low-order gravity field coefficients with the tracked (>1 h duration) 17F12v2 flybys of Case Study 1 in Scenario 2, as a function of DSN configuration (Table 10). Entries in bold indicate that the requirement (rightmost column) was not met.

Parameter	DSN_{34m} (26 flybys)	$DSN_{2\times34m}$ (26+5=31 flybys)	$DSN_{3\times34m}$ (26+5+5=36 flybys)	DSN_{70m} (26+5+5+3=39 flybys)	Requirement
k_2	**0.075**	0.055	0.049	0.046	<0.06
$\bar{C}_{20}$	$\mathbf{9.0 \times 10^{-6}}$	6.6×10^{-6}	6.0×10^{-6}	5.6×10^{-6}	$<8.0 \times 10^{-6}$
$\bar{C}_{22}$	$\mathbf{15 \times 10^{-6}}$	$\mathbf{11 \times 10^{-6}}$	$\mathbf{9.5 \times 10^{-6}}$	$\mathbf{9.0 \times 10^{-6}}$	$<9.0 \times 10^{-6}$
$\bar{C}_{30}$	$\mathbf{33 \times 10^{-7}}$	$\mathbf{26 \times 10^{-7}}$	$\mathbf{21 \times 10^{-7}}$	$\mathbf{18 \times 10^{-7}}$	$<4.0 \times 10^{-7}$
$\bar{C}_{40}$	$\mathbf{31 \times 10^{-7}}$	$\mathbf{27 \times 10^{-7}}$	$\mathbf{20 \times 10^{-7}}$	$\mathbf{16 \times 10^{-7}}$	$<4.0 \times 10^{-7}$

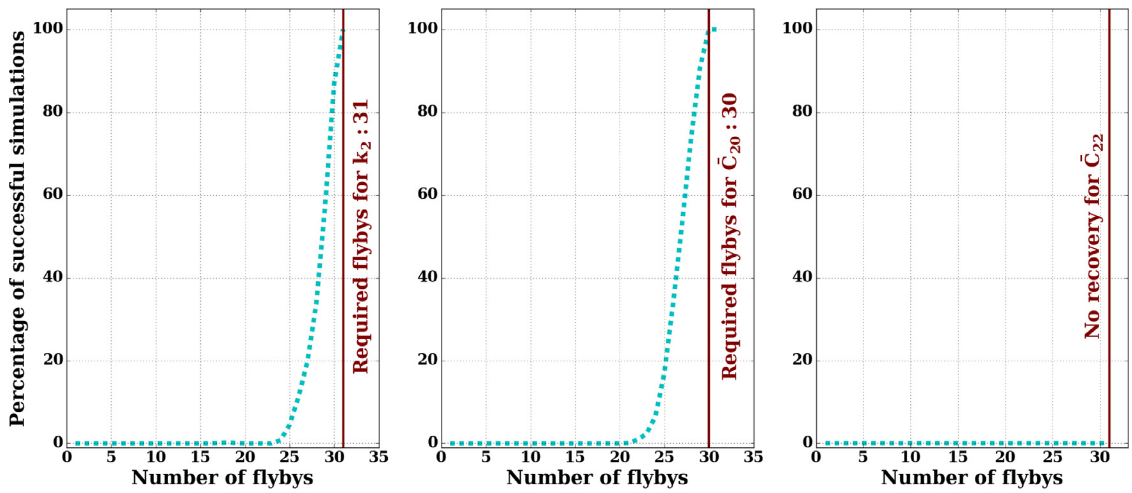

Fig. 10. Percentage of simulations that meet the tidal Love number k_2 and gravity field coefficients $\bar{C}_{20}$ and $\bar{C}_{22}$ measurement objectives, when considering up to 10,000 sets of randomly selected, tracked (>1 h duration), 17F12v2 flybys, as a function of the number of flybys considered in the sets (Scenario 2, Case Study 2). Simulations include both Doppler and crossover measurements and incorporate tracking of up to 31 flybys with the $DSN_{2\times34m}$ antenna configuration (26 flybys tracked with a single 34 m antenna and 5 additional flybys tracked with a 2x34 m antenna array), excluding high-altitude (>100 km) and low SEP (<20°) flybys.

Table 13
Observed latitudinal distribution of 17F12v2 flybys in successful simulations, i.e., in simulations where sets of randomly selected flybys always met the tidal Love number k_2 and $\bar{C}_{20}$ gravity field coefficients measurement objectives (Scenario 2, Case Study 2). The measurement objective for $\bar{C}_{22}$ was never achieved. Simulations include both Doppler and crossover measurements and incorporate tracking of up to 31 flybys with the $DSN_{2\times34m}$ antenna configuration (26 flybys tracked with a single 34 m antenna and 5 additional flybys tracked with a two-antenna array), excluding high-altitude (>100 km) and low SEP (<20°) flybys. The rightmost columns indicate the medians and standard deviations of the number of flybys that were included in successful simulations.

Europa region	Latitude range	Available flybys	k_2	$\bar{C}_{20}$	$\bar{C}_{22}$
High latitude north	90° – 45°	7	7 ± 0	6 ± 1	...
Mid latitude north	45° – 15°	4	4 ± 0	4 ± 0	...
Low latitude	15° – −15°	13	13 ± 0	13 ± 0	...
Mid latitude south	−15° – −45°	5	5 ± 0	5 ± 0	...
High latitude south	−45° – −90°	2	2 ± 0	2 ± 0	...
Total	90° – −90°	31	31	30	...

We found that it is possible to meet the k_2 and $\bar{C}_{20}$ measurement objectives 100% of the time with 31 and 30 randomly chosen flybys, respectively. The measurement objective for $\bar{C}_{22}$ was never achieved (Fig. 10). The counter-intuitive result of meeting the k_2 ($\bar{C}_{20}$) measurement objectives with 31 (30) flybys in this scenario versus 34 (33) flybys in the Case Study 2 of Scenario 1 (Section 5.1.2) is due to the fact that, in Scenario 2, a larger proportion of equatorial flybys is represented in the pool of 31 flybys than in the pool of 39 flybys in Scenario 1. Equatorial flybys provide a better determination of k_2 than high-latitude flybys.

As in Scenario 1, we identified the latitudinal distribution of flybys in successful simulations. (Table 13).

5.2.3. Case study 3: preferred sets of flybys

In this third and final case study for Scenario 2, we examined the number of tracked (>1 h duration) flybys required to meet the k_2 measurement objective with careful selection of the flybys according to latitude region. As shown in Section 5.2.1, a single 34 m antenna is not sufficient to meet this objective. Therefore we selected the $DSN_{2\times34m}$ antenna configuration (Table 10) to perform this case study with 31 tracked flybys.

As in Section 5.1.3, we started with all low-latitude flybys and gradually increased the number of randomly selected mid- and high-latitude flybys until the measurement objective was achieved.

We found that it is possible to meet the k_2 measurement objective with 25 flybys (Table 14, Fig. 11), as long as they include all 13 low-latitude flybys, at least 8 mid-latitude flybys, and at least 4 high-latitude flybys. This result applies to the 17F12v2 trajectory

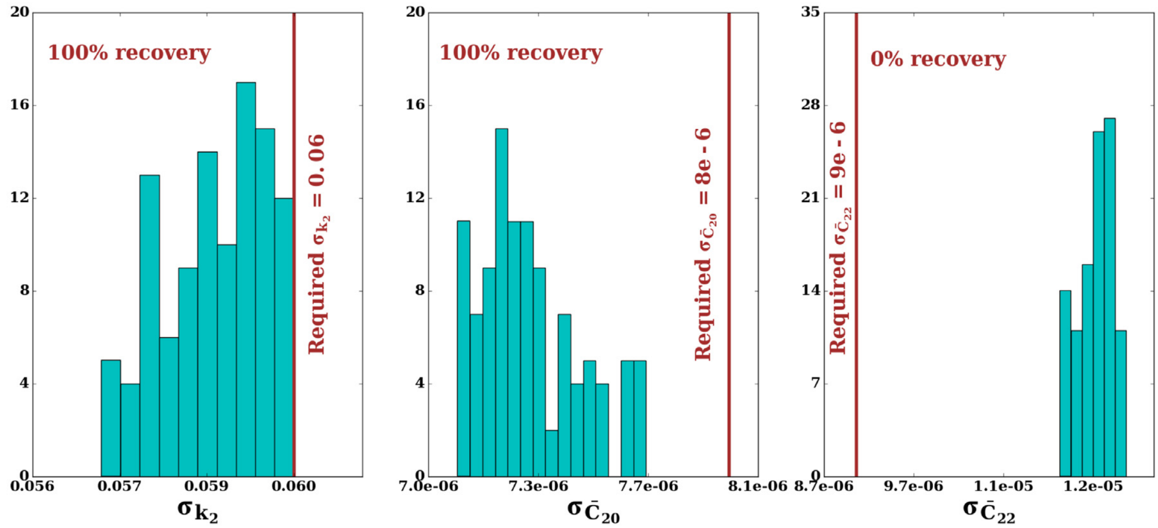

Fig. 11. Histograms of k_2, $\bar{C}_{20}$, and $\bar{C}_{22}$ uncertainties obtained by performing covariance analyses for all possible combinations of 25 flybys using the $DSN_{2\times34m}$ antenna configuration with the latitudinal distribution shown in Table 14 (Scenario 2, Case Study 3).

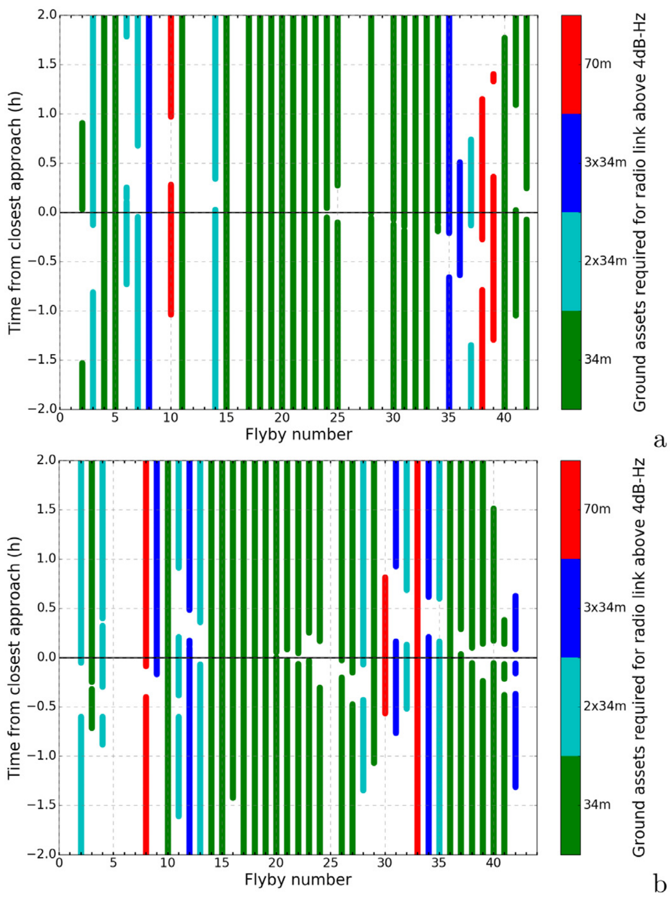

Fig. 12. Time intervals during which a 4 dB-Hz radio link can be maintained for at least 1 h with trajectories 15F10 (left) and 16F11 (right). For each flyby, the least sensitive antenna configuration was used, resulting in the following 15F10 configuration: 23 tracks with a 34 m antenna (green), 5 tracks with a 2×34 m array (cyan), 3 tracks with a 3×34 m array, and 3 tracks with a 70 m antenna (red) for 15F10. For 16F11, the configuration includes 22 tracks with a 34 m antenna (green), 7 tracks with a 2×34 m array (cyan), 5 tracks with a 3×34 m array (blue), and 3 tracks with a 70 m antenna (red). Flybys with low SEP angle (<20°) or high altitude (> 100 km) were discarded.

Table 14
Number of methodically selected 17F12v2 mid- and high-latitude flybys required to meet the tidal Love number k_2 measurement objective when flybys are tracked with the $DSN_{2\times34m}$ antenna configuration and all low-latitude flybys are tracked (Scenario 2, Case Study 3).

Europa region	Latitude range	Avail. flybys	Req. flybys
High latitude north	90° – 45°	7	2
Mid latitude north	45° – 15°	4	4
Low latitude	15° – −15°	13	13
Mid latitude south	−15° – −45°	5	4
High latitude south	-45° – −90°	2	2
Total	90° – −90°	31	25

and $DSN_{2\times34m}$ antenna configuration. The measurement objective for $\bar{C}_{20}$ is also met, but that of $\bar{C}_{22}$ is never met for any combination of 25 flybys. Failure to track a single low-latitude flyby from the 13 available in 17F12v2 would result in a failure to meet Clipper's primary gravity science objective. This fact highlights an element of risk associated with relying on the $DSN_{2\times34m}$ antenna configuration. This risk is reduced when using 70 m antennas.

6. Other trajectories

In an attempt to generalize our results, we examined the suitability of the other trajectories available to us, 15F10 and 16F11, for meeting the k_2 measurement objective. The 15F10 and 16F11 trajectories consist of 42 and 43 flybys, respectively. They yield 88 and 106 illuminated crossover points below 1000 km altitude, respectively. Similar to Scenario 2 of trajectory 17F12v2 (Section 5.2), Doppler observations were simulated with the least sensitive DSN configuration that maintains the 4dB-Hz radio link budget for track durations of at least 1 h. Fig. 12 shows the time intervals for which such a link can be maintained with a variety of DSN assets within ±2 h of closest approach. After further discarding flybys with SEP angle <20° and closest approach altitude >100 km, a total of 34 and 37 tracked flybys remain with the 15F10 and 16F11 trajectories, respectively. The numbers of Doppler and crossover measurements that can be obtained with the available flybys are shown in Table 15.

Similar to the first case study in Scenario 2 (Section 5.2.1), we examined the precision of the Love number k_2 as data from consecutive flybys becomes available. We found that the k_2 measurement objective is not achievable with a single 34 m antenna

Table 15
Number of Doppler and crossover measurements that can be obtained with trajectories 15F10 and 16F11 with various DSN configurations. The number of crossovers corresponds to the number of intersections of tracked flybys. The number of tracked flybys are shown in columns 2 and 5. Also shown are the total durations (columns 4 and 7) during which tracking can be conducted with a link budget above 4 dB-Hz, expressed as a fraction of the total potential tracking time (± 2 h of each closest approach). Flybys with <1 h tracking duration, SEP angle <20°, and altitude >100 km were discarded.

DSN config.	15F10				16F10			
	Tracked flybys	Doppler msr.	Crossover msr.	Tracking fraction	Tracked flybys	Doppler msr.	Crossover msr.	Tracking fraction
DSN_{34m}	23	5065	35	50%	22	4808	30	47%
$DSN_{2\times34m}$	23+5	5844	46	58%	22+7	6052	59	59%
$DSN_{3\times34m}$	23+5+3	6367	51	63%	22+7+5	6834	74	66%
DSN_{70m}	23+5+3+3	6774	68	67%	22+7+5+3	7377	85	71%

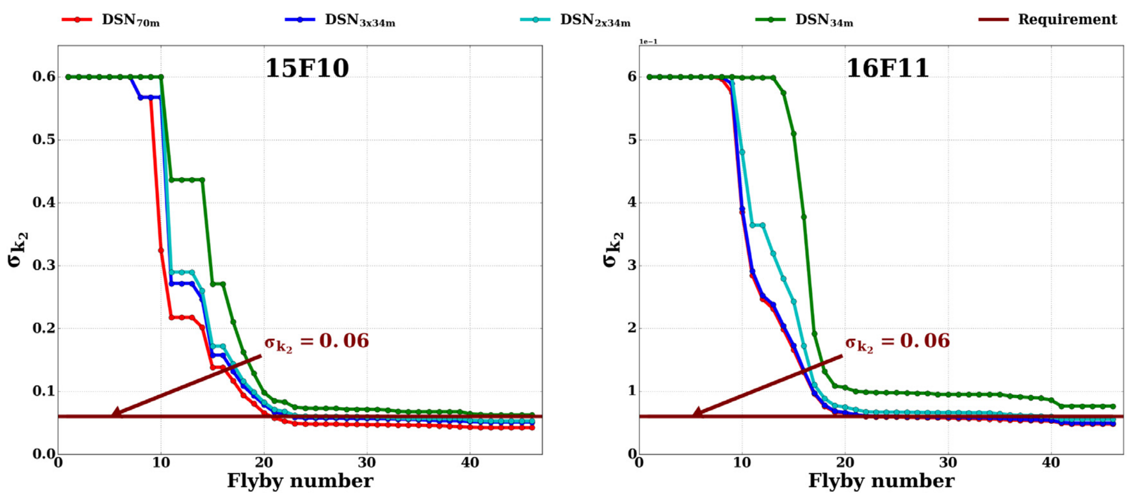

Fig. 13. Precision of the tidal Love number k_2 when data from 42(43) consecutive flybys of 15F10(16F11) trajectory are analyzed (flybys with <1 h tracking duration, SEP angle <20°, and altitude >100 km were discarded) using progressively more sensitive DSN configurations (Fig. 12). The green curve shows the performance with a single 34 m antenna using a total of 23 (22) flybys (DSN_{34m}). The cyan curve considers the addition of a 2×34 m antenna array for 5 (7) flybys, a total of 28 (29) flybys ($DSN_{2\times34m}$). The blue curve considers the addition of a 3×34 m antenna for 3 (5) flybys, a total of 31 (34) flybys ($DSN_{3\times34m}$). The red curve considers the addition of a single 70 m antenna for 3 (3) flybys, a total of 34 (37) flybys ($DSN_{2\times34m}$) and is nearly indistinguishable from the blue curve in the case of the 16F11 trajectory. The brown horizontal lines indicate the measurement objectives specified in Table 1.

Table 16
Estimated uncertainties in tidal Love number k_2 and low-order gravity field coefficients for trajectories 15F10 and 16F11 when 28 and 29 flybys, respectively, are tracked (duration > 1 h) with the $DSN_{2\times34m}$ antenna configuration. Entries in bold indicate that the requirement (rightmost column) was not met.

Parameters	$DSN_{2\times34m}$		Requirement
	15F10	16F11	
k_2	0.053	0.055	<0.06
$\bar{C}_{20}$	6.0×10^{-6}	6.6×10^{-6}	$<8.0 \times 10^{-6}$
$\bar{C}_{22}$	$\mathbf{10 \times 10^{-6}}$	$\mathbf{11 \times 10^{-6}}$	$<9.0 \times 10^{-6}$
$\bar{C}_{30}$	$\mathbf{30 \times 10^{-7}}$	$\mathbf{29 \times 10^{-7}}$	$<4.0 \times 10^{-7}$
$\bar{C}_{40}$	$\mathbf{31 \times 10^{-7}}$	$\mathbf{27 \times 10^{-7}}$	$<4.0 \times 10^{-7}$

(Fig. 13). However, as in the situation with the 17F12v2 trajectory, the k_2 measurement objective can be met (Table 16) with both 15F10 and 16F11 trajectories and $DSN_{2\times34m}$ antenna configurations, where the majority of flybys are tracked with a single 34 m antenna and a few additional flybys are tracked with a 2×34 m antenna array (Table 15).

We also examined the minimum number and latitudinal distribution of tracked flybys that are required to meet the k_2 measurement objective. We selected the $DSN_{2\times34m}$ antenna configuration (Table 15) to perform this case study with 28 and 29 tracked flybys for trajectories 15F10 and 16F11, respectively. We selected the flybys as in Case Study 3 of Scenario 2 (Section 5.2.3).

We found that a minimum of 24 flybys with a specific latitudinal distribution (Table 17) are sufficient to meet the k_2 measurement objective for both trajectories. As with the 17F12v2 trajectory, the measurement objective for $\bar{C}_{20}$ is also met with the same distribution of flybys, whereas the measurement objective for $\bar{C}_{22}$ is never met for any combination of 24 flybys.

In summary, it takes at least 24 carefully selected flybys in 15F10 and 16F11 (Table 17) and at least 25 carefully selected flybys in 17F12v2 (Table 14) to meet the k_2 objective with the $DSN_{2\times34m}$ antenna configuration. The similarity in the required number of flybys suggests that it may be possible to generalize the results to other trajectories that are similar in character (Section 7).

7. Generalized tracking requirements

Here, we examine whether results that apply to trajectories 15F10, 16F11, and 17F12v2 are sufficiently similar that they can be extrapolated to other trajectories that are similar in character. Our results are summarized in Table 18. Taking the maximum values of these results as a basis for extrapolation, we find that a minimum of ∼13 low-latitude, ∼8 mid-latitude, and ∼5 high-latitude flybys are necessary to meet the k_2 objective. Likewise, we find that a total tracking duration that is at least 50% of the total potential tracking time (± 2 h of each closest approach) is necessary. Expressed as a fraction of total potential tracking time for selected flybys only (tracking duration >1 h, altitude <100 km, SEP angle >20° deg), the required percentage is 88%. The availability of at least 52 crossover points in illuminated regions completes the requirements.

Table 17
Minimum number of flybys required in each latitude band to meet the tidal Love number k_2 measurement objective with the 15F10 and 16F11 trajectories when flybys are tracked with the $DSN_{2\times 34m}$ antenna configuration.

Europa region	Latitude range	15F10		16F11	
		Avail. flybys	Req. flybys	Avail. flybys	Req. flybys
High latitude north	90° − 45°	7	3	4	2
Mid latitude north	45° − 15°	5	5	7	7
Low latitude	15° − −15°	11	11	12	12
Mid latitude south	−15° − −45°	3	3	4	1
High latitude south	−45° − −90°	2	2	2	2
Total	90° − −90°	28	24	29	24

Table 18
Summary of results obtained with 15F10, 16F11, and 17F12v2 trajectories and the $DSN_{2\times 34m}$ antenna configuration. Tracking fraction refers to the total duration during which tracking can be conducted with a link budget above 4 dB-Hz, expressed as a fraction of the total potential tracking time (±2 h of each closest approach). Flybys with <1 h tracking duration, SEP angle <20°, and altitude >100 km were discarded.

Europa region	Trajectory								
	15F10			16F11			17F12v2		
	No. of flybys	Tracking fraction	No. of crossovers	No. of flybys	Tracking fraction	No. of crossovers	No. of flybys	Tracking fraction	No. of crossovers
High latitude: 90° − 45°	5			4			4		
Mid latitude: 15° − 15°	8	50%	38	8	49%	50	8	47%	52
Low latitude: 15° − 0°	11			12			13		
Total	24	50%	38	24	49%	50	25	47%	52

8. Conclusions

A Europa Clipper gravity science investigation can address important mission objectives, such as confirming the presence of an ocean, determining Europa's gravity field, quantifying the time-varying tidal potential, verifying whether the ice shell is hydrostatic, and providing high-precision reconstructed trajectories that other instrument teams will greatly benefit from.

We performed covariance analyses to quantify the precision with which geophysical parameters can be determined with a radio science investigation and a nominal mission profile with trajectory 17F12v2. We found that the availability of crossover measurements allows measurement objectives to be achieved with substantially fewer tracked flybys than in a Doppler-only scenario. Even with 70 m antennas, the measurement objective for the second degree and order gravitational harmonic cannot be achieved without crossover measurements.

By simulating hundreds of thousands of combinations of tracked flybys, we were able to quantify the distribution of flybys with sub-spacecraft latitudes at closest approach within certain latitude regions that provides the best prospects for meeting measurement objectives. We found that tracking a dozen low-latitude flybys and a dozen mid- to high-latitude flybys are both essential.

We found that it is not possible to maintain a 4 dB-Hz radio link budget during a ±2 h interval centered on each flyby's closest approach epoch, even with the most sensitive ground-based assets of the DSN. However, we found that 45 out of 46 flybys can be tracked for a total duration of at least one hour with a 70 m antenna. With a 34 m antenna, 26 out of 46 flybys can be tracked for a total duration of at least one hour, and 5 additional flybys can be tracked for a total duration of at least one hour with a two-antenna array of 34 m diameter antennas.

If 70 m antennas are used, the tidal Love number k_2 measurement objective can be met by tracking at least 23 methodically selected flybys, with good resilience in case certain flybys are unexpectedly missed. If 34 m antennas are used without arraying, the k_2 measurement objective is not achievable. However, it is achievable by tracking 26 flybys with 34 m antennas and 5 additional flybys with arrays of two 34 m antennas. If flybys are carefully selected with respect to the latitudinal distribution of closest approaches, the k_2 objective can be met by tracking at least 25 flybys with 34 m antennas and two-antenna arrays, provided that all low-latitude flybys are tracked. Such a configuration provides little margin for error.

By comparing our 17F12v2 results to 15F10 and 16F11 results, we showed that our conclusions are roughly generalizable to trajectories that are similar in character.

Acknowledgments

AKV and JLM were supported in part by NASA Europa Mission Project Subcontract 1569162. This work was enabled in part by the Mission Operations and Navigation Toolkit Environment (MONTE) and the Spacecraft, Planet, Instrument, Camera-matrix, Events (SPICE) toolkit. MONTE and SPICE are developed at the Jet Propulsion Laboratory, which is operated by Caltech under contract with NASA. The Europa Clipper trajectory data used in this work is available from the NAIF server at ftp://naif.jpl.nasa.gov/pub/naif/EUROPACLIPPER. We thank James Roberts and Robert Pappalardo with assistance in specifying gravity science measurement requirements. We thank Dipak Srinivasan, Peter Ilott, Avinash Sharma, and Ryan Park with assistance in providing values of system parameters. We thank Gregor Steinbrügge for providing estimates of range uncertainties at crossover locations. We thank Francis Nimmo for providing helpful comments on the manuscript and GSWG members for informative discussions.

Supplementary material

Supplementary material associated with this article can be found, in the online version, at doi:10.1016/j.icarus.2018.05.018.

References

Acton, C., Bachman, N., Semenov, B., Wright, E., 2017. A look towards the future in the handling of space science mission geometry. Planet. Space Sci. doi:10.1016/j.pss.2017.02.013.

Anderson, J.D., Schubert, G., Jacobson, R.A., Lau, E.L., Moore, W.B., Sjogren, W.L., 1998. Europa's differentiated internal structure: inferences from four Galileo encounters. Science 281, 2019. doi:10.1126/science.281.5385.2019.

Archinal, B.A., A'Hearn, M.F., Bowell, E., Conrad, A., Consolmagno, G.J., Courtin, R., Fukushima, T., Hestroffer, D., Hilton, J.L., Krasinsky, G.A., Neumann, G., Oberst, J., Seidelmann, P.K., Stooke, P., Tholen, D.J., Thomas, P.C., Williams, I.P., 2011. Report of the IAU working group on cartographic coordinates and rotational elements: 2009. Celestial Mech. Dyn. Astron. 109, 101–135.

Asmar, S.W., Armstrong, J.W., Iess, L., Tortora, P., 2005. Spacecraft Doppler tracking: noise budget and accuracy achievable in precision radio science observations. Radio Sci. 40, RS2001. doi:10.1029/2004RS003101.

Bierman, G.J., 1977. Factorization Methods for Discrete Sequential Estimation, 128. Academic Press, New York, NY, p. 241. 1977

Bills, B.G., Nimmo, F., Karatekin, Ö., van Hoolst, T., Rambaux, N., Levrard, B., Laskar, J., 2009. Rotational Dynamics of Europa. In: Pappalardo, R.T., McKinnon, W.B., Khurana, K.K. (Eds.), Europa. University of Arizona Press, p. 119.

Blankenship, D.D., Moussessian, A., Schroeder, D.M., Soderlund, K.M., Grima, C., Gim, Y., Plaut, J.J., Schmidt, B.E., 2014. Flyby sounding of Europa's icy shell: radar investigations, analogs, and instruments for the Europa Clipper mission. In: Workshop on the Habitability of Icy Worlds, 1774, p. 4053.

Deep Space Network, 2016. DSN Telecommunications Link Design Handbook 810-005. Technical Report. Jet Propulsion Laboratory.

Evans, S., Taber, W., Drain, T., Smith, J., Wu, H.C., Guevara, M., Sunseri, R., Evans, J., 2016. MONTE: the next generation of mission design & navigation software. In: The 6th International Conference on Astrodynamics Tools and Techniques (ICATT).

Gravity Science Working Group, 2016. Report of the Gravity Science Working Group for the Europa Multiple Flyby Mission. Technical Report. National Aeronautics and Space Agency.

Greenberg, A.H., Margot, J.-L., Verma, A.K., Taylor, P.A., Naidu, S.P., Brozovic, M., Benner, L.A.M., 2017. Asteroid 1566 Icarus's size, shape, orbit, and Yarkovsky drift from radar observations. Astron. J. 153, 108. doi:10.3847/1538-3881/153/3/108.

Iess, L., Benedetto, D.M., Marabucci, M., Racioppa, P., 2012. Improved Doppler tracking systems for deep space navigation. In: Proceedings of the 23rd edition of the International Symposium on Space Flight Dynamics (ISSFD), Pasadena.

Iess, L., Rappaport, N.J., Jacobson, R.A., Racioppa, P., Stevenson, D.J., Tortora, P., Armstrong, J.W., Asmar, S.W., 2010. Gravity field, shape, and moment of inertia of Titan. Science 327, 1367. doi:10.1126/science.1182583.

Kaula, W.M., 2000. Theory of Satellite Geodesy: Applications of Satellites to Geodesy. Dover Publications.

Konopliv, A.S., Asmar, S.W., Folkner, W.M., Karatekin, Ö., Nunes, D.C., Smrekar, S.E., Yoder, C.F., Zuber, M.T., 2011. Mars high resolution gravity fields from MRO, Mars seasonal gravity, and other dynamical parameters. Icarus 211, 401–428. doi:10.1016/j.icarus.2010.10.004.

Konopliv, A.S., Banerdt, W.B., Sjogren, W.L., 1999. Venus gravity: 180th degree and order model. Icarus 139, 3–18.

Lam, T., Arrieta-Camachoy, J.J., Buffington, B.B., 2015. The Europa mission: multiple Europa flyby trajectory design trades and challenges. Technical Report. Jet Propulsion Laboratory, Pasadena, California.

Lieske, J.H., 1998. Galilean satellite ephemerides E5. Astron. Astrophys. Suppl. Ser. 129, 205–217. doi:10.1051/aas:1998182.

Margot, J.-L., Padovan, S., Campbell, D., Peale, S., Ghigo, F., 2013. Measurements of the spin states of Europa and Ganymede. In: AAS/Division for Planetary Sciences Meeting Abstracts. In: AAS/Division for Planetary Sciences Meeting Abstracts, 45, p. 504.02.

Mazarico, E., Genova, A., Neumann, G.A., Smith, D.E., Zuber, M.T., 2015. Simulated recovery of Europa's global shape and tidal love numbers from altimetry and radio tracking during a dedicated flyby tour. Geophys. Res. Lett. 42, 3166–3173. doi:10.1002/2015GL063224.

Mazarico, E., et al., 2014. The gravity field, orientation, and ephemeris of Mercury from MESSENGER observations after three years in orbit. J. Geophys. Res. (Planets).

McCarthy, D.D., Petit, G., 2004. IERS Conventions (2003). IERS Technical Note 32.

Moore, W.B., Schubert, G., 2000. NOTE: the tidal response of Europa. Icarus 147, 317–319. doi:10.1006/icar.2000.6460.

Moyer, T.D., 2003. Formulation for observed and computed values of deep space network data types for navigation, 2. John Wiley & Sons.

NASA DSN, 2017. DSN Telecommunications Link Design Handbook (810-005, Rev. E, Change 42). Technical Report. Jet Propulsion Laboratory.

National Research Council, 1999. A Science Strategy for the Exploration of Europa. National Academies Press doi:10.17226/9451.

National Research Council, 2011. Vision and Voyages for Planetary Science in the Decade 2013–2022. National Academies Press doi:10.17226/13117.

Pappalardo, R.T., Senske, D.A., Korth, H., Blankenship, D., Blaney, D., Christensen, P., Kempf, S., Raymond, C., Retherford, K., Turtle, E.P., Waite, J.H., Westlake, J., Collins, G.C., Hand, K., Lunine, J., McGrath, M., Nimmo, F., Paty, C., Soderblom, J., Spencer, J.R., Paranicas, C., Solomon, S., Europa Science Team, 2017. The Europa multiple-flyby mission: synergistic science to investigate habitability. In: Lunar and Planetary Science Conference, 48, p. 2732.

Park, R.S., Asmar, S.W., Buffington, B.B., Bills, B., Campagnola, S., Chodas, P.W., Folkner, W.M., Konopliv, A.S., Petropoulos, A.E., 2011. Detecting tides and gravity at Europa from multiple close flybys. Geophys. Res. Lett. 38, L24202. doi:10.1029/2011GL049842.

Park, R.S., Bills, B., Buffington, B.B., Folkner, W.M., Konopliv, A.S., Martin-Mur, T.J., Mastrodemos, N., McElrath, T.P., Riedel, J.E., Watkins, M.M., 2015. Improved detection of tides at Europa with radiometric and optical tracking during flybys. Planet. Space Sci. 112, 10–14. doi:10.1016/j.pss.2015.04.005.

Sjogren, W.L., Banerdt, W.B., Chodas, P.W., Konopliv, A.S., Balmino, G., Barriot, J.P., Arkani-Hamed, J., Colvin, T.R., Davies, M.E., 1997. The Venus gravity field and other geodetic parameters. In: Venus II: Geology, Geophysics, Atmosphere, and Solar Wind Environment, p. 1125.

Smith, D.E., Sjogren, W.L., Tyler, G.L., Balmino, G., Lemoine, F.G., Konopliv, A.S., 1999. The gravity field of Mars: results from Mars Global Surveyor. Science 286, 94–97. doi:10.1126/science.286.5437.94.

Smith, D.E., Zuber, M.T., Phillips, R.J., Solomon, S.C., Hauck, S.A., Lemoine, F.G., Mazarico, E., Neumann, G.A., Peale, S.J., Margot, J.-L., Johnson, C.L., Torrence, M.H., Perry, M.E., Rowlands, D.D., Goossens, S., Head, J.W., Taylor, A.H., 2012. Gravity field and internal structure of mercury from MESSENGER. Science 336, 214–217.

Steinbrügge, G., Schroeder, D.M., Haynes, M.S., Hussmann, H., Grima, C., Blankenship, D.D., 2018. Assessing the potential for measuring Europa's tidal love number h_2 using radar sounder and topographic imager data. Earth Planet. Sci. Lett. 482, 334–341. doi:10.1016/j.epsl.2017.11.028.

Turtle, E.P., McEwen, A.S., Collins, G.C., Fletcher, L., Hansen, C.J., Hayes, A.G., Hurford, T.A., Kirk, R.L., Barr Mlinar, A.C., Nimmo, F., Patterson, G.W., Quick, L.C., Soderblom, J.M., Thomas, N., Ernst, C.M., 2016. The Europa Imaging System (EIS): high-resolution imaging and topography to investigate Europa's geology, ice shell, and potential for current activity. In: Lunar and Planetary Science Conference, 47, p. 1626.

Verma, A.K., Margot, J.L., 2016. Mercury's gravity, tides, and spin from MESSENGER radio science data. J. Geophys. Res. (Planets) 121, 1627–1640. doi:10.1002/2016JE005037.

Verma, A.K., Margot, J.-L., Greenberg, A.H., 2017. Prospects of dynamical determination of general relativity parameter β and solar quadrupole moment $J_{2\odot}$ with asteroid radar astronomy. Astrophys. J. 845, 166. arXiv: 1707.08675.doi:10.3847/1538-4357/aa8308.

Wahr, J.M., Zuber, M.T., Smith, D.E., Lunine, J.I., 2006. Tides on Europa, and the thickness of Europa's icy shell. J. Geophys. Res. (Planets) 111, E12005. doi:10.1029/2006JE002729.